Core scattering of quadratic Zeeman orbits in barium

Hong-Ping Liu,[1,2,*] Wei Quan,[1,2,3] Li Shen,[1,2,3] Jean-Patrick Connerade,[4,1] and Ming-Sheng Zhan[1,2]
[1]*State Key Laboratory of Magnetic Resonance and Atomic and Molecular Physics, Wuhan Institute of Physics and Mathematics, Chinese Academy of Sciences, Wuhan 430071, People's Republic of China*
[2]*Center for Cold Atom Physics, Chinese Academy of Sciences, Wuhan 430071, People's Republic of China*
[3]*Graduate School of Chinese Academy of Sciences, Beijing 100080, People's Republic of China*
[4]*Quantum Optics and Laser Science Group, The Blackett Laboratory, Imperial College, London SW7 2BW, United Kingdom*
(Received 24 April 2007; published 19 July 2007)

We report a method to uncover the peaks due to scattering of quadratic Zeeman orbits by the atomic core of a many-electron atom. The method is experimental, and consists in identifying the supernumerary peaks in the scaled-energy spectra by comparing them with the corresponding hydrogenic calculations using closed-orbit theory. The scaled actions of the observed additional peaks correspond to combining the scaled actions of individual closed orbits, except for a small blueshift, which is explainable as a core-induced interaction, depending on the penetration of the orbits. Our method is related to earlier theoretical studies of helium, but can be applied to any experimentally accessible atom, including those with large cores. We show that, for barium, core-scattering processes do indeed occur, and that they are confined to a specific portion of the scaled-energy spectrum.

DOI: 10.1103/PhysRevA.76.013412 PACS number(s): 32.60.+i, 32.30.Jc, 34.60.+z, 32.80.Cy

I. INTRODUCTION

Rydberg atoms in high magnetic fields have played a central role in the study of small quantum systems with classically chaotic underlying dynamics. This problem has a long and distinguished history, beginning with the discovery of the quadratic Zeeman effect (QZE) in barium [1] and culminating in the experiments of Welge and co-workers on atomic hydrogen [2]. The motivation for these early experiments was to explore how the correspondence principle connects the spectrum of the simplest nonseparable quantum system to the dynamics of its classical counterpart.

More recently, the interest has shifted to the study of many-electron atoms. This arose from certain features of closed-orbit theory (COT), a method that describes the dynamics of Rydberg atoms in strong external fields in terms of classical orbits closed at the nucleus [3–5]. It was discovered that scattering of the Rydberg electron by an atomic core gives rise to combination orbits which are not seen in hydrogen. As a result, in nonhydrogenic systems, one expects effects associated with classically forbidden orbits to be far more important than they are in hydrogen through the intrusion of different orbits due to core scattering and mixing [6].

Consequently, a number of authors [7–15] have steered the subject toward the study of atoms, and even of molecules [16], containing an electronic core. Such studies have involved not only experiment, but also theory. Hüpper, Main, and Wunner modeled the ionic core by means of a pseudopotential in order to investigate the scattering of classical orbits in helium with pure external magnetic fields [8], while Rao, Delande, and Taylor performed the first quantum calculation of the scaled spectrum of a nonhydrogenic atom in crossed fields [9].

More recently still, Zhao and Du [14] combined standard COT away from the core region with close-coupling R-matrix theory inside the core to search for signatures of inelastic (interchannel) scattering of active electrons by the atomic core. The method used was entirely theoretical: by turning on and turning off the interaction in their calculation and comparing the resulting spectra, they were able to uncover features corresponding to combinations of closed orbits originating from different channels.

In the present paper, we describe an experimental extension based on a similar principle to search for inelastic scattering by the atomic core in quadratic Zeeman spectra. Rather than work with light atoms, a choice dictated by the complexity of performing the relevant calculations, we are free to select *any* experimentally accessible atom. We have therefore chosen to reconsider barium, first, because it has a very large core, and second, because there is a strong and well-documented interaction between the Rydberg series $6s^2\ ^1S_0 \rightarrow 6snp\ ^1P_1$ and doubly excited core states $5d8p\ ^{1,3}P_1$ [17,18], a situation that can arise only for the heavy alkaline-earth metal elements. Thus, in addition to the type of scattering encountered in He, there is the possibility of involving excited states of the core, whose influence on the Rydberg states is already strong. Our method consists in measuring the scaled-energy spectrum experimentally, and then comparing the result, feature by feature, with hydrogenic COT calculations. It is found that additional features are indeed observed in our experiment, and that these features all match expected energies for "mixed" states produced by scattering off the core.

In the course of our work, we have also performed a scaled-energy study of the quadratic Zeeman effect in barium. Although the QZE was actually discovered in barium, which has been studied by a number of authors since [19–28], it seems that other aspects of the spectroscopy were involved in all of the earlier experiments. In the present paper, we report spectra for barium in magnetic fields at the scaled energies $\varepsilon = -2.240$, -1.300, -0.900, -0.800, and -0.700.

*Corresponding author. liuhongping@wipm.ac.cn

 ©2007 The American Physical Society

II. CLOSED-ORBIT THEORY IN A MAGNETIC FIELD

The Hamiltonian of a hydrogen atom with energy E in a uniform magnetic field along the z axis, in cylindrical coordinates, is

$$H = \frac{1}{2}p_\rho^2 + \frac{1}{2}p_z^2 + \frac{l_z^2}{2\rho^2} - \frac{1}{\sqrt{\rho^2+z^2}} + \frac{1}{8}\gamma^2\rho^2, \tag{1}$$

where γ is the magnetic field in atomic unit, defined as $\gamma = B/c = B/2.35\times 10^5$ with B in tesla.

We define a set of scaled variables as follows:

$$\hat{q} = \frac{q}{2}\gamma^{2/3}, \quad \hat{p} = p\gamma^{-1/3}, \quad \hat{t} = \frac{t}{2}\gamma, \quad \hat{H} = H\gamma^{-2/3}, \tag{2}$$

and write the scaled Hamiltonian $\hat{H}$ as

$$\hat{H} = \frac{1}{2}\left(\hat{p}_\rho^2 + \hat{p}_z^2 + \frac{\hat{l}_z^2}{\hat{\rho}^2} - \frac{1}{\sqrt{(\hat{\rho}^2+\hat{z}^2)}} + \hat{\rho}^2\right), \tag{3}$$

where $\hat{l}_z$ is the z component of angular momentum scaled by $\hat{l}_z = l_z\gamma^{-1/3}$. When considering the classical dynamics of the above system in scaled coordinates, we find that, for $\hat{l}_z = 0$, the classical dynamics of the scaled Hamiltonian in Eq. (3) does not depend on the energy E and magnetic field strength B separately, but solely on one parameter, the scaled energy ε, where

$$\varepsilon = E\gamma^{-2/3}. \tag{4}$$

So if we control the scaled energy ε in Eq. (4) to be constant by matching the exciting photon energy and the magnetic field at the same time, the classical dynamics of the atoms will be held invariant while, experimentally, we can record the absorption spectrum by scanning the excitation photon energy, which provides dynamical information about the outer electron. This procedure is successfully incorporated into the closed-orbit theory developed by Du and Delos [5]. According to this theory, the photon absorption rate is related to the average oscillator-strength density $\overline{Df}(E,B)$, which can be written as a combination of a smooth background term and a set of sinusoidal oscillations,

$$\overline{Df}(E,B) = \overline{Df_0}(E) + \overline{Df_{osc}}(E,B), \tag{5}$$

where the smooth background term $\overline{Df_0}(E)$ is the basic oscillator strength in the absence of magnetic field while the second term $\overline{Df_{osc}}(E,B)$ is the contribution of the oscillations in the magnetic field. Defining

$$\omega = 2\pi\gamma^{-1/3}, \tag{6}$$

the latter oscillatory part $\overline{Df_{osc}}(E,B)$ can be written as

$$\overline{Df_{osc}}(E,B) = \sum_n (2\pi)^{1/2}\omega^{-1/2}D_0^n(\varepsilon)\sin[\hat{S}_0^n(\varepsilon)\omega - \Phi_0] + \sum_{n,k} D_k^n(\varepsilon)\sin[\hat{S}_k^n(\varepsilon)\omega - \Phi_{nk}], \tag{7}$$

where $D_0^n(\varepsilon)$ and $D_k^n(\varepsilon)$ are the amplitudes of the nth repetition of the kth closed orbit for different initial conditions, i.e., $\theta_i = 0$ and $\theta_i \neq 0$, $\hat{S}_0^n(\varepsilon)$ and $S_k^n(\varepsilon)$ are their scaled actions, and Φ_0 and $\Phi_{k,n}$ are their phase shifts, which are determined by their Maslov indices. In calculations, it must be noted that the maximum action is confined by the experimentally accessible precision $\Delta\omega$ according to the formula $S \leq 2\pi/\Delta\omega$. In our experiment, the resolvable maximum action $S \leq 15$, which means that longer closed orbits cannot be resolved under our conditions.

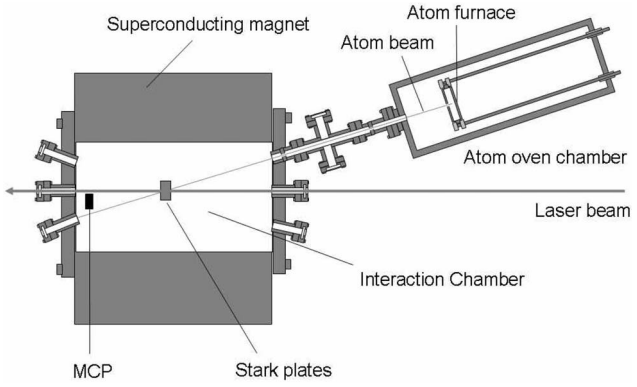

FIG. 1. Experimental sketch of our apparatus for scaled-energy spectroscopy in a magnetic field. The atom beam is produced by resistively heating a barium furnace with an alternating current around 80–120 A and is aligned with two pinholes to a direction of a small angle of 15° to the magnetic field. The interaction area is well shielded and connected to the ionization area by a copper mesh 4 mm in diameter (not shown).

III. EXPERIMENT

Our experimental apparatus, as shown schematically in Fig. 1, consists essentially of two parts. One is the atomic source chamber where the atom beam is produced, and the other is the interaction chamber, where the atom beam interacts with the laser beam under the influence of the magnetic field. The atomic oven, shaped as a cylinder, is made of nickel-chromium alloy. In the front side of the atomic oven is a pinhole with diameter about 0.7 mm. When a current of about 80–120 A is applied to it, the oven will be resistively heated to temperature up to 500 °C, and the barium sample inside begins to produce vapor, which is ejected from the pinhole. The beam is defined by a pair of 20-cm-separated pinholes (around 5 mm in diameter), and then arrives in the interaction chamber where it is irradiated by the laser in the geometric center of the magnet, between a pair of Stark plates. The laser beam is aligned along the axes of the magnet while the atom beam is aligned crossing the magnetic field at a small angle of 15°, in a geometry similar to that of Drinkwater *et al.* [29] but with the directions interchanged. This configuration reduces the motional Stark effect to a degree that can be neglected, compared with the laser linewidth in our experiment. The Stark plates are originally designed for crossed-field experiments, and here we just use them to compensate the motional Stark effect by applying an appropriate electric field, although this effect is very small in our case.

The pulsed laser used in our experiment is generated by a yttrium aluminum garnet pumped Lambda Physik Scanmate 2E dye laser system where an étalon is inserted in the cavity to narrow the linewidth down to 1.2 GHz. The energy of each pulse is around 1 mJ. The laser beam from the dye laser is frequency doubled by a system-controlled β-BaB_2O_4 crystal and the dichromatic beams are separated by a pair of prisms. The fundamental laser frequency is monitored by a Burleigh wavemeter. A step-motor-driven Soleil-Babinet compensator is used to convert the laser from linear to circular polarization actively during the wavelength scanning. One photon (around 238.5 nm) excites the barium atom from the ground state to Rydberg states. A set of spectra in free field was acquired to compare with the published spectral lines [30] and thereby to calibrate our laser frequency. The superconducting magnet (Oxford Instruments) can produce magnetic fields up to 5.5 T in the central area of the chamber and sweep with stability better than 1 G. The laser light is intentionally scattered a little by the chamber and shielding components to make a fast signal on the multichannel plate (MCP) before the ionized atom arrives. We used this signal to monitor the laser intensity and normalize the spectral signal. The MCPs are arranged perpendicular to the magnetic field and located near the vacuum chamber end, where the magnetic field has already been reduced a lot so as to achieve the best detection efficiency. The resulting ionic signal is transferred via a screened cable to an oscilloscope (Tektronix TDS 1012) and then downloaded into a PC to keep the whole wave form for further data processing, which is much better than using solely a boxcar integrator instead [31].

During the experiment, the computer controlled the dye laser system and the superconducting magnet at the same time to keep the scaled energy $\varepsilon = E\gamma^{-2/3}$ constant, as described in the previous section of the paper. The principal quantum number n varies from 28 to 55, in which range the states are perturbed by the $5d8p$ state. The motional Stark effect is actively canceled by applying an appropriate electric field [31].

In our experiment, the superconducting magnet can sweep with very high stability, and the main experimental uncertainty comes from the laser bandwidth and the scanning fluctuations. The induced uncertainty on the scaled energy is dependent on the wavelength and magnetic field according to Eq. (4). At a wavelength 238.5±1.0 nm and in magnetic fields 0.163 32–1.853 35 T for our case, the uncertainties of the scaled energy at $\varepsilon = -2.240$, -1.300, -0.900, -0.800, and -0.700 were reduced from 0.007 to 0.001. For simplicity, the recurrence spectrum is obtained by performing a general Fourier transform for the experimental scaled-energy spectrum instead of by the chirped Fourier transform [2] or the harmonic inversion method [32]. A cutoff function has been used in our data processing [33].

IV. RESULTS AND DISCUSSION

The barium spectra are recorded at several different scaled energies $\varepsilon = -2.240$, -1.300, -0.900, -0.800, and -0.700, in our experiment, with the corresponding $\gamma^{-1/3}$ varying in the ranges 51.1–112.3, 66.8–86.0, 54.0–69.1, 51.1–65.4, and 47.8–61.0, respectively. The principal quantum number concerned varies between 28 and 55 for $\varepsilon = -2.240$ and between 46 and 55 for other scaled energies. The experimental results are presented in Figs. 2–4, where the scaled-energy spectra at $\varepsilon = -2.240$ were acquired with both σ^+ and σ^- circularly polarized laser beams and those at the other energies only for the σ^+ transition.

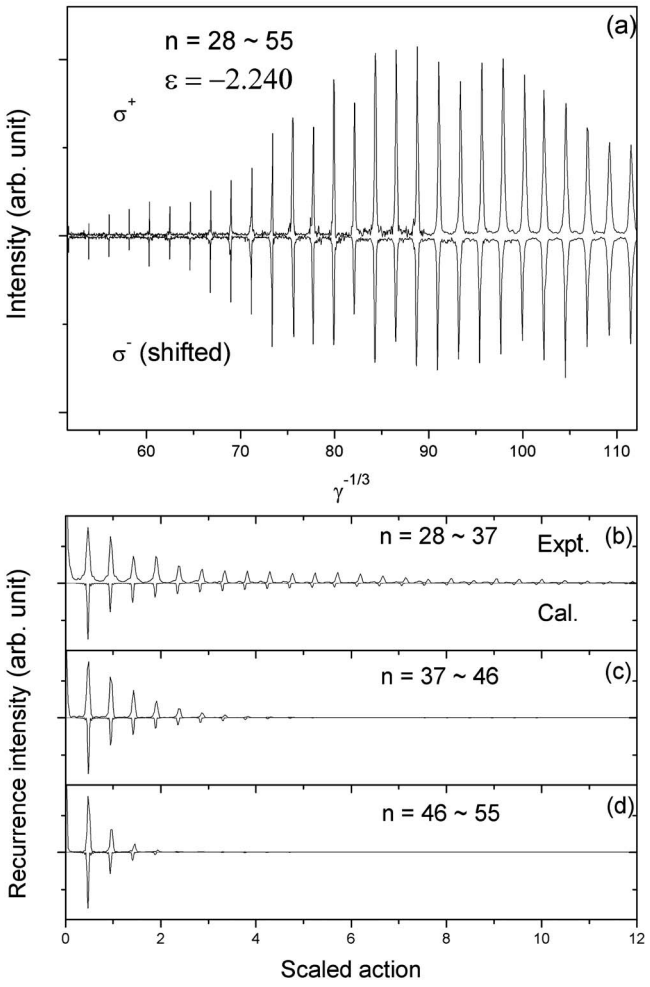

FIG. 2. Spectrum of barium at scaled energy $\varepsilon = -2.240$. (a) is the comparison of σ^+ and σ^- scaled energy spectra at $\varepsilon = -2.240$ with cancellation of the motional Stark effect. The σ^- spectrum has been shifted for comparison. The upward pointing parts of (b)–(d) are recurrence spectra by Fourier transformation of the experimental data for the σ^+ transition of (a) in different principal quantum number ranges 28–37, 37–46, and 46–55, respectively. The downward pointing parts are peaks calculated by the closed-orbit theory for a hydrogen atom with a cutoff function inserted [33].

As depicted in Fig. 2(a), we first obtained the scaled energy spectra at $\varepsilon = -2.240$ for both σ^+ and σ^- circularly polarized lasers to make sure that the motional Stark effect has been canceled. The spectrum for σ^- is shifted to compare with that for σ^+, which corresponds to an energy change of γ in atomic units. It can be seen that the two sets of spectral lines coincide very well, but the spectral intensity for σ^- is slightly smaller than for the σ^+ branch. This is probably due to the fact that higher photon energy is required to irradiate

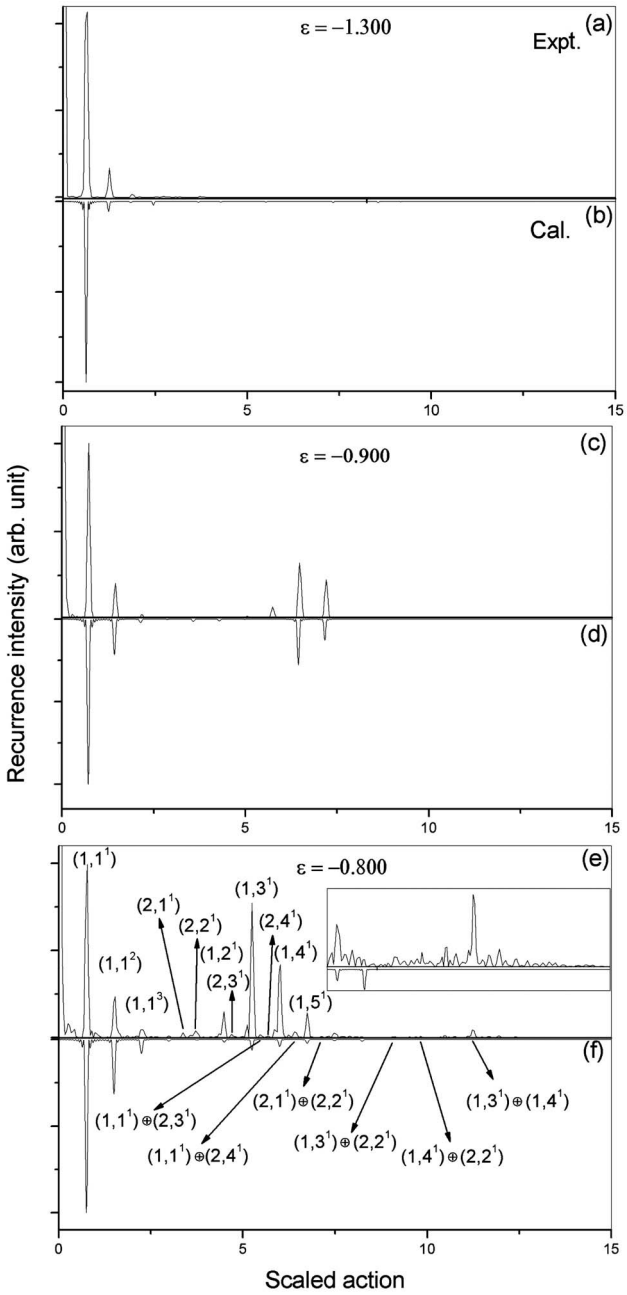

FIG. 3. Experimental recurrence spectrum for barium at scaled energies $\varepsilon=-1.300$, -0.900, and -0.800 within $n=46-55$ (a),(c),(e) and the corresponding one calculated by closed-orbit theory for hydrogen (b),(d),(f). Obviously, a new recurrence peak comes out at the large action of 11.25 without a hydrogen counterpart (e). It is assumed to be the sum of the combination of orbits at $S=5.25$ and $S=6.00$ due to intrachannel scattering events, denoted by $(1,3^1)\oplus(1,4^1)$. Another new peak at 7.13 is also identified and assumed to be the mixing of $S=3.38$ and $S=3.73$ but neither of them has one-electron closed-orbit correspondence in our calculation. It should be the closed orbit in a different quantum channel due to the state mixing from the perturbation $5d8p$. These are indicated by $(2,1^1)\oplus(2,2^1)$. In addition, interchannel scattering between different quantum channels is also observed, indicated as $(1,1^1)\oplus(2,3^1)$, $(1,1^1)\oplus(2,4^1)$, $(1,3^1)\oplus(2,2^1)$, and $(1,4^1)\oplus(2,2^1)$ (see the text for details).

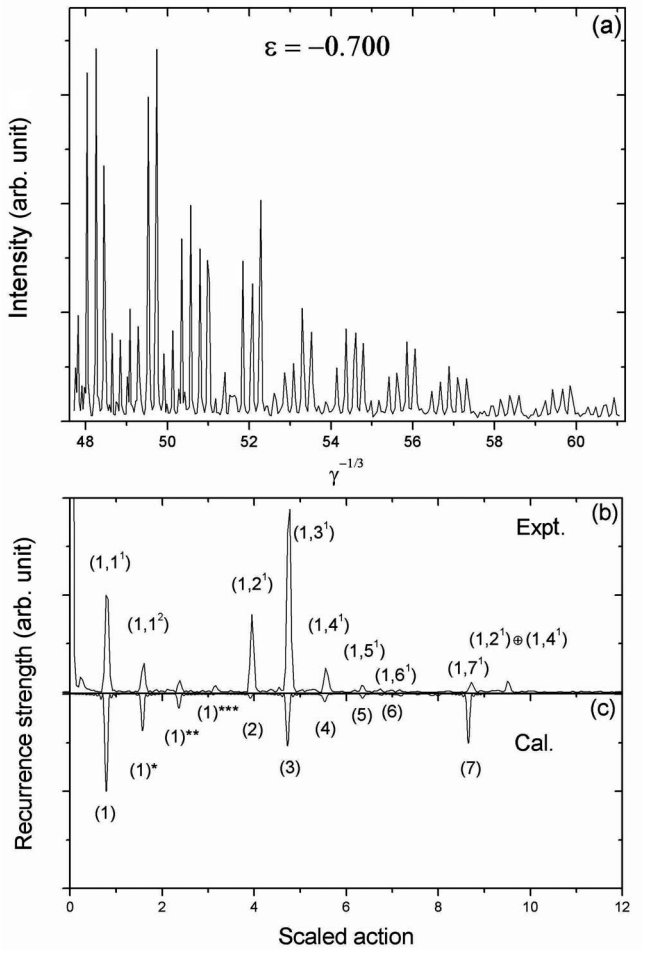

FIG. 4. Experimental scaled energy spectrum for barium at $\varepsilon=-0.700$ in the range of $n=46-55$ (a) and its corresponding recurrence spectrum by Fourier transform (b) in comparison with the calculated by closed orbit theory for hydrogen (c). A new combination orbit is observed at 9.51, indicated by $(1,2^1)\oplus(1,4^1)$ in (b).

the σ^- transition. Another interesting fact is that the spectral linewidth gets wider and wider with increasing $\gamma^{-1/3}$, from $\Delta\gamma=0.032$ at $\gamma^{-1/3}=60.0$ to $\Delta\gamma=0.405$ at $\gamma^{-1/3}=110.0$. The main contribution for the broadening is the uncertainty transferred from the laser linewidth and its scanning fluctuation, scaled by the magnetic field intensity following Eq. (4).

In Figs. 2(b)–2(d), the experimental recurrence spectra at $\varepsilon=-2.240$ in different principal quantum number ranges 28–37, 37–46, and 46–55 were compared with the closed orbit calculation for hydrogen, corrected by a cutoff function. This function is tuned by the uncertainties of scaled energy at every photon energy range, considering the experimental resolution. The corresponding uncertainties of scaled energy were 0.001–0.003, 0.003–0.005, and 0.004–0.007, respectively. For $n=46-55$, the estimated uncertainty of scaled energy approximately equals the one used in our calculation (0.0073), while large deviations were found in comparison with those for $n=28-37$ and 37–46. The estimated uncertainties of scaled energy for these two ranges were 0.003 and 0.005. To study the recurrence maps and their different features at different scaled energies, we choose the spectrum

within the same photon energy range, i.e., $n=46-55$, for investigation, which will be seen in the following parts.

In comparison to the experimental recurrence spectra for barium and closed-orbit recurrence spectra for hydrogen, we found that the actions of recurrence peaks of barium were always a little larger than those calculated for hydrogen, especially at large scaled action areas. As we can see from Figs. 2(b)–2(d), at $\varepsilon=-2.240$, in the range $n=28-37$, the calculated actions of the peaks are 97.72% of those observed, while within $n=37-46$ the deviation becomes larger and larger, reaching 96.22%. The biggest deviation occurs at $n=46-55$ with 95.24%. We can also see this feature even at high scaled energy, i.e., $\varepsilon=-0.700$ (see Fig. 4). Additionally, a closed-orbit calculation shows that at this scaled energy only perpendicular orbits and their repetitions exist, as we have observed. However, the number of repetitions is determined by the experimental resolution. We can observe more than 20 repetitions at $n=28-37$ [in Fig. 2(b)], many more than that at $n=37-46$ [in Fig. 2(d)], where only a few repetitions are found.

The increasing deviations of the scaled action of recurrence peaks we observed is similar to the results of the recurrence spectroscopic investigation in electric field by Bates *et al.* [21]. As in their analysis, the deviations are due to the energy dependence of the quantum defect for the Rydberg states. Barium has a quantum defect of 4.2 for a p state around $n=55$, varying from 4.148 at $n=50$ to 4.240 at $n=60$. This energy dependence of the quantum defect for the Rydberg series has the consequence that the peaks at large-magnitude-scaled actions shift from their one-electron locations. In particular, the barium core had a strong shadowing effect for long orbits, which will be clearly seen below in the case of the scaled energy recurrence spectroscopy at $\varepsilon=-0.700$.

The dependence of the recurrence spectrum within $n=46-55$ on scaled energy is given in Fig. 3. The first closed orbit, the perpendicular orbit, and its repetition do not change much with the scaled energy. However, when the scaled energy increases to $\varepsilon=-0.900$, several new orbits appear around the scaled action $S=6.50$, and are well consistent with the closed-orbit calculation for hydrogen. When ε reaches -0.800, there are more peaks, extending to the range between 3.3 and 7.2. Unlike the recurrence spectrum at $\varepsilon=-0.900$, the amplitudes of the recurrence peaks between 5.2 and 7.2 are much stronger than the calculated ones for hydrogen. An interesting point is that there are several peaks that have no counterpart for the calculated spectrum. They are scattered at $S=3.38$, 3.73, 4.70, 5.47, 5.65, 6.47, 7.13, and 11.25, denoted as $(2,1^1)$, $(2,2^1)$, $(2,3^1)$, $(1,1^1)\oplus(2,3^1)$, $(2,4^1)$, $(1,1^1)\oplus(2,4^1)$, $(2,1^1)\oplus(2,2^1)$, and $(1,3^1)\oplus(1,4^1)$, in Fig. 3(e), respectively, and will be explained below.

Following the notation by Zhao and Du [14], we denote the hydrogen closed orbits for a specific core quantum state as (ζ,k^n), where ζ stands for a channel of the quantum states and k and n denote a closed orbit and its repetition, and the notation $(\zeta_1,k_1^{n_1})\oplus(\zeta_2,k_2^{n_2})$ represents a combination of closed orbits. If ζ_1 and ζ_2 are the same, we call this kind of combination an intrachannel event, corresponding to elastic scattering from one hydrogen closed orbit to another without changing the core state. If ζ_1 and ζ_2 are different, the combination will mean an inelastic scattering event between interchannel events with core state exchange. In our case, careful analysis found that the peak at 11.25 should be the sum of the combination of orbits at $S=5.25$ and $S=6.00$, labeled by $(1,3^1)$ and $(1,4^1)$. These core-scattered mixing orbits are also observed in the recurrence spectrum of helium [34] and lithium [35]. The observed combination closed orbit at 11.25 should be due to the elastic scattering by the core, since its child peaks can be reproduced by the hydrogen closed-orbit calculation [14]. We denote this core state as channel I. Another new peak at 7.13 is assumed to be the mixing of $S=3.38$ and $S=3.73$ but neither of them has one-electron closed-orbit correspondence in our calculation. The combination is labeled by $(2,1^1)\oplus(2,2^1)$ in Fig. 3(e). By analogy with the calculations for the recurrence spectra of He atom in a magnetic field by Zhao and Du [14], we speculate that these child orbits are from another quantum channel, denoted as channel II, due to the mixing of the perturbation state(s) concerned with $5d8p$, which is not included in our calculation. However, we can make sure that they also obey the closed-orbit calculation for hydrogen but for different quantum core state(s). Besides the observation of the elastic core scattering between intrachannel events, we have also observed inelastic interchannel core scattering, although it is very weak. The recurrence peaks at large scaled actions are magnified in the inset in Fig. 3(e), where we can see that the peak at $S=9.73$ should be the mixing of orbits at 6.00 and 3.73, denoted as $(1,4^1)\oplus(2,2^1)$, and the one at $S=9.06$ the mixing of orbits at 5.25 and 3.73, denoted as $(1,3^1)\oplus(2,2^1)$, between interchannel events, although the latter has a small deviation from the sum 8.98. More inelastic interchannel core-scattering orbits can be found. They are denoted as $(1,1^1)\oplus(2,3^1)$ at $S=5.47$ and $(1,1^1)\oplus(2,4^1)$ at $S=6.47$. These combination orbits between channels I and II also convince one of the existence of a perturber state.

In particular, we present the scaled energy spectrum at $\varepsilon=-0.700$ in Fig. 4 to analyze its orbits in more detail. Figure 4(a) is the experimental scaled energy spectrum at $\varepsilon=-0.700$ and Fig. 4(b) the recurrence spectrum of Fig. 4(a) by Fourier transform. The spectrum calculated by closed-orbit theory for hydrogen is also presented for comparison, displayed as downward peaks in Fig. 4(c). It can be seen in Fig. 4(b) that the first peak is the perpendicular orbit and the following three are its repetitions, in agreement with the calculation by closed orbits for a one-electron atom core. Where the scaled action is around 5.00, the intensities of experimental peaks 2–4 are much larger than the calculated ones, and their peak positions are also shifted to the blue side of the calculated ones. More deviation is found at $S=8.70$ for peak 7. Unlike the recurrence peaks 2–4, the amplitude for peak 7 is depressed several times, compared with the calculated ones. This shows that core scattering can reinforce or weaken the stabilities of the closed orbits efficiently. As in Fig. 3(e) at $\varepsilon=-0.800$, there still exists a new recurrence peak ($S=9.51$), corresponding to a new closed orbit, although its amplitude is small. It is easily found that this recurrence peak is a combination of the closed orbits at $S=3.96$ and 5.55, as

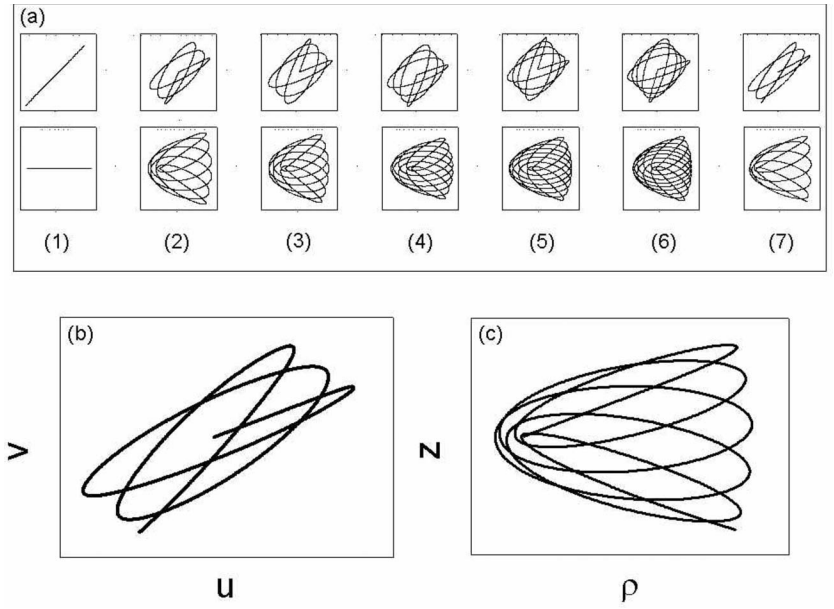

FIG. 5. Closed orbits calculation for hydrogen atom at scaled energy $\varepsilon=-0.700$. The corresponding orbits for peaks in Fig. 4 are drawn in coordinate systems $u-v$ and $\rho-z$ (a) and specifically the magnified orbit for the 7th is redrawn in (b) and (c) for careful observation.

indicated by $(1,2^1)\oplus(1,4^1)$. This means that there exists a rescattering from one orbit to another by intrachannel interaction [14]. However, no interchannel recurrence peak is observed at this scaled energy. It seems to indicate that the perturber moves far away from the hydrogenlike core of barium at this moment.

The closed orbits corresponding to the recurrence peaks in Fig. 4(c) are displayed in u-v and ρ-z coordinates, respectively, in Fig. 5. An interesting observation is that, as the action increases, the evolving electron will approach the core more and more closely during its closed trip. An obvious conclusion can be drawn that the closed orbit with larger action will be influenced by the core more easily, and naturally its recurrence amplitude and closed-orbit period will change greatly, at the same time. The closed snake orbit for peak 7 is specially redrawn in Figs. 5(b) and 5(c) for careful study. The closeness of its approach to the core may well be the reason that peak 7 deviates from the calculated parameters and has a depressed amplitude. This gives a strong hint that a higher-resolution experiment could unveil the core effects more accurately.

V. CONCLUSION

We have measured the scaled-energy spectra for barium at several scaled energies in a magnetic field. From these scaled-energy spectra, we were able, by comparing the experimental data with hydrogenic COT calculations, to identify a number of inelastic scattering events involving interchannel mixing due to core scattering. An interesting result is that all the peaks that were uncovered by our procedure were found in the scaled-energy range corresponding to $\varepsilon=-0.800$, which suggests that the interchannel scattering is particularly strong around this value.

Our method is a straightforward extension to experiment of the theoretical technique initiated by Zhao and Du [14]. However, we are able (i) to apply it to any experimentally accessible atom (including systems with a large core) and (ii) to pick out energy ranges in the Rydberg spectrum where perturbations due to core-excited states play an important role. A blueshift of the recurrence peaks was also observed, in agreement with the results of previous work for barium in an electric field [21], but in a different excitation configuration. Additionally, the general feature emerged that recurrence peaks are reinforced or depressed as compared with the closed-orbit calculation for the hydrogenic system.

Finally, we stress that our method is quite general: in principle, any atom with a core can be explored in this way, and the reference hydrogenic closed-orbit calculations used for comparison are the simplest ones to perform, and essentially the same for all Rydberg atoms. However, should the number of mixed channels become large, there might be difficulty in deciding which closed orbits are contributing. We have not encountered this difficulty in our study even for an element as complex as barium.

ACKNOWLEDGMENTS

This work is supported by National Natural Science Foundation of China (NNSFC) under Grants No. 10404033 and No. 10474119. We are grateful for support from the Royal Society of London and the Chinese Academy of Sciences in the form of a Joint Project (No. 16455). We would also like to thank H. C. Jia, H. Z. Zhang and J. R. Li for their technical supports.

[1] W. R. S. Garton and F. S. Tomkins, Astrophys. J. **158**, 839 (1969).
[2] S. Freund, R. Ubert, E. Flöthmann, K. Welge, D. M. Wang, and J. B. Delos, Phys. Rev. A **65**, 053408 (2002).
[3] M. L. Du and J. B. Delos, Phys. Rev. A **38**, 1913 (1988).
[4] M. L. Du and J. B. Delos, Phys. Rev. A **38**, 1896 (1988).
[5] M. L. Du and J. B. Delos, Phys. Rev. Lett. **58**, 1731 (1987).
[6] A. Matzkin, P. A. Dando, and T. S. Monteiro, Phys. Rev. A **67**, 023402 (2003).
[7] B. Hüpper, J. Main, and G. Wunner, Phys. Rev. A **53**, 744 (1996).
[8] B. Hüpper, J. Main, and G. Wunner, Phys. Rev. Lett. **74**, 2650 (1995).
[9] J. Rao, D. Delande, and K. T. Taylor, J. Phys. B **35**, L1 (2002).
[10] K. Karremans, A. Kips, W. Vassen, and W. Hogervorst, Phys. Rev. A **60**, R2649 (1999).
[11] K. Weibert, J. Main, and G. Wunner, Ann. Phys. (N.Y.) **268**, 172 (1998).
[12] P. A. Dando, T. S. Monteiro, D. Delande, and K. T. Taylor, Phys. Rev. A **54**, 127 (1996).
[13] M. Hoffmann-Ostenhof and T. Hoffmann-Ostenhoft, J. Phys. A **17**, 3321 (1984).
[14] L. B. Zhao and M. L. Du, Phys. Lett. A **363**, 453 (2007).
[15] M. Keeler and T. J. Morgan, Phys. Rev. Lett. **80**, 5726 (1998).
[16] A. Matzkin, M. Raoult, and D. Gauyacq, Phys. Rev. A **68**, 061401(R) (2003).
[17] J. P. Connerade and A. M. Lane, Rep. Prog. Phys. **51**, 1439 (1988).
[18] J. P. Connerade and A. M. Lane, J. Phys. B **18**, L605 (1985).
[19] J. P. Connerade, S. D. Hogan, and A. M. Abdulla, J. Phys. B **38**, S141 (2005).
[20] A. M. Abdulla, S. Hogan, M. S. Zhan, and J.-P. Connerade, J. Phys. B **37**, L147 (2004).
[21] K. A. Bates, J. Masae, C. Vasilescu, and D. Schumacher, Phys. Rev. A **64**, 033409 (2001).
[22] A. Kips, W. Vassen, and W. Hogervorst, J. Phys. B **33**, 109 (2000).
[23] J.-P. Connerade, G. Droungas, N. E. Karapanagioti, and M. S. Zhan, J. Phys. B **30**, 2047 (1997).
[24] G. J. Kuik, A. Kips, W. Vassen, and W. Hogervorst, J. Phys. B **29**, 2159 (1996).
[25] R. J. Elliott, G. Droungas, and J.-P. Connerade, J. Phys. B **28**, L537 (1995).
[26] G. Droungas, N. E. Karapanagioti, and J.-P. Connerade, Phys. Rev. A **51**, 191 (1995).
[27] A. König, J. Neukammer, K. Vietzke, M. Kohl, H. J. Grabka, H. Hieronymus and, H. Rinneberg, Phys. Rev. A **38**, 547 (1988).
[28] R. J. Fonck, F. L. Roesler, D. H. Tracy, K. T. Lu, F. S. Tomkins, and W. R. S. Garton, Phys. Rev. Lett. **39**, 1513 (1977).
[29] K. J. Drinkwater, J. Hormes, D. D. Burgess, J. P. Connerade, and R. C. M. Learner, J. Phys. B **17**, L439 (1984).
[30] W. R. S. Garton and F. S. Tomkins, Astrophys. J. **158**, 839 (1969).
[31] W. Quan, H.-P. Liu, L. Shen, and M.-S. Zhan, Chin. Phys. Lett. **24**, 672 (2007).
[32] J. A. Shaw and F. Robicheaux, Phys. Rev. A **58**, 3561 (1998).
[33] J. Main, G. Wiebusch, K. Welge, J. Shaw, and J. B. Delos, Phys. Rev. A **49**, 847 (1994).
[34] D. Delande, K. T. Taylor, M. H. Halley, T. van der Veldt, W. Vassen, and W. Hogervorst, J. Phys. B **27**, 2771 (1994).
[35] M. Courtney, H. Jiao, N. Spellmeyer, and D. Kleppner, Phys. Rev. Lett. **73**, 1340 (1994).